A Dual Cobalt-Photoredox Catalytic Approach for Asymmetric Dearomatization of Indoles with Aryl Amides *via* C-H Activation

Abir Das,[a] Subramani Kumaran,[a] Harihara Subramanian Ravi Sankar,[a] J. Richard Premkumar,[b] and Basker Sundararaju[a]*

[a] A. Das, Dr. S. Kumaran, H. S. Ravi Sankar, Prof. Dr. B. Sundararaju
Department of chemistry,
Indian Institution of Technology Kanpur,
Kanpur, Uttar Pradesh, India – 208 016.
E-mail: basker@iitk.ac.in

[b] J. R. Prem Kumar
PG & Research Department of Chemistry,
Bishop Heber College,
Tiruchirappalli-620017, Tamil Nadu, India.

Supporting information for this article is given via a link at the end of the document.((Please delete this text if not appropriate.))

Abstract: In this study, we unveil a novel method for the asymmetric dearomatization of indoles under cobalt/photoredox catalysis. By strategically activating C-H bonds of amides and subsequent migratory insertion of π-bonds present in indole as reactive partner, we achieve *syn*-selective tetrahydro-5*H*-indolo[2,3-*c*]isoquinolin-5-one derivatives with excellent yields and enantiomeric excesses of up to >99%. The developed method operates without a metal oxidant, relying solely on oxygen as the oxidant and employing an organic dye as a photocatalyst under irradiation. Control experiments and stoichiometric studies elucidate the reversible nature of the enantiodetermining C-H activation step, albeit not being rate-determining. This study not only expands the horizon of cobalt-catalyzed asymmetric C-H bond functionalization, but also showcases the potential synergy between cobalt and photoredox catalysis in enabling asymmetric synthesis of complex molecules.

Introduction

Faraday's serendipitous discovery of benzene unveiled the doorway to a realm of molecules that would shape the course of modern chemistry.[1] Over the past decade, the annual production of aromatic scaffolds has reached up to 100 million tons. Therefore, there has been a concerted effort to harness the abundant reservoir of flat aromatic molecules and elevate them into value-added, three-dimensional, complex molecular architectures.[2-5] However, due to unparallel stability[6-8] offered by the aromatic compounds through delocalization of π-electrons within their molecular framework empowers them to engage in a myriad of chemical transformations while preserving their aromatic character.[9-10] Alternatively, uncovering strategies to disrupt aromaticity presents a promising avenue for generating novel molecular frameworks from widely available aromatic hydrocarbons.[11-12] Besides traditional approaches,[13-17] hydrogenation,[18] nucleophilic addition[19] mediated by transition metals, and selective 1,2-hydroxylation mediated by enzymes[20] are among the known examples in the literature. In recent years, catalytic asymmetric dearomatization reactions have gained prominence as a potent synthetic methodology to access complex molecular architectures.[2-3],[5] This approach facilitates the transformation of various π-bonds present in the aromatic compounds as a reactive functional group, thereby enabling their utilization in creation of chiral molecules. Among the aromatic scaffolds, phenol and its derivatives,[11],[21-23] indole,[12] and other heteroarenes[24] have been extensively used in asymmetric dearomatization *via* cyclo addition,[19] allylic substitution,[25] hydrogenation,[18] arenophile-mediated dearomatization,[26] etc. However, Activation of inert C-H bond and subsequent coupling of π-bonds that involved in aromaticity is seldom explored.[27-29] In this regard, You and co-workers reported the novel chiral Cp#Rh-catalyzed asymmetric dearomatization of 2-naphthols with alkyne *via* ortho-C-H bond activation of the 1-phenyl-2-naphthol derivatives.[27,28] Xu and Lu recently reported the cascade intramolecular C-C and C-H activation strategy catalyzed by Rh(I)/(*S*)-dtbm-Segphos to access complex tetra cyclic core.[29]

On the other hand, The field of cobalt-catalyzed C-H bond functionalization has witnessed remarkable expansion since the seminal work by Daugulis,[30] particularly in the realm of bidentate-directing group-assisted transformations.[31] Recent developments have witnessed a shift towards sustainable methodologies, with investigations into the replacement of traditional oxidants like Mn(III) or Ag(I) with photocatalysts under irradiation[32b-d] or utilizing electricity as the sole oxidant.[32a-b]

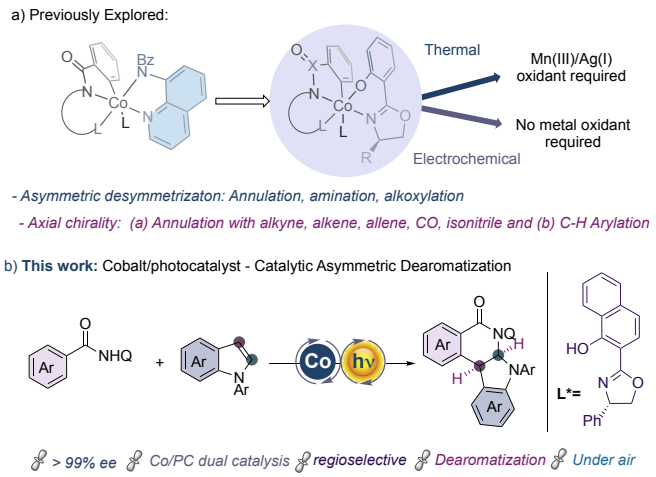

Scheme 1. Overview of Ligand enabled Co(III) catalysis and asymmetric C-H bond functionalizations.

Additionally, a profound understanding of the active octahedral cobaltacycles[33] formed in-situ has led to breakthroughs in asymmetric catalysis facilitated by the use of simple cobalt(II) salts and enantiopure Salox ligands as chiral sources.[34-35] This novel strategy has been explored led by Shi, Ackermann and Niu in cobalt-catalyzed asymmetric C-H bond functionalizations encompassing diverse transformations such as annulation with alkynes, alkenes, allenes, isonitriles as well as C-H arylation, under both thermal and electrochemical conditions.[36] Furthermore, the topic has been explored for asymmetric desymmetrization of phosphinamides through C-C, C-O and C-N bond formation with alkynes, alcohols, amines under mild conditions.[37]

To the best of our knowledge, the asymmetric desymmetrization of indoles coupled with C-H activation catalyzed by cobalt remains unexplored. Furthermore, utilization of a photocatalyst under irradiation to supplant the stoichiometric quantities of Mn(III) or Ag(I) in cobalt(II)-catalyzed asymmetric C-H bond functionalizations has not been documented. However, it is noteworthy that electricity has been successfully employed as a sole oxidant in these contexts for asymmetric C-H bond functionalization with cobalt, circumventing the need for Mn(III) and Ag(I).[36b], [36e], [36h], [37c-e] Previously, our research effort have achieved notable advancements in C-H bond annulation and alkynylation by synergistically employing cobalt and photocatalyst under oxidant-free conditions, resulting in racemic products.[32d] Notably, these efforts have yielded successful outcomes with alkyne, alkene, and bromoalkyne substrates.[38],[39] However, the transition to an asymmetric variant using the cobalt/PS dual catalytic approach has remained a formidable challenge. This challenge arises due to the lack of systematic validation of chiral ligands and the intricate interplay between the photocatalyst and the enantio-determining step. In this study, we unveil the novel method for the asymmetric dearomatization of indole. This process involves the enantio-determining C-H bond activation of amides, followed by the migratory insertion of the π-bond of the indole, essential for preserving aromaticity under cobalt/photoredox catalysis. This strategic approach results in the synthesis of *syn*-selective tetrahydro-5*H*-indolo[2,3-*c*]isoquinolin-5-one derivatives in excellent yields, with enantiomeric excess reaching up to >99%.

Results and Discussion

In our pursuit of achieving enantioselective dearomatization of indoles through C-H and N-H bond annulation strategies, we initiated our preliminary investigation employing *N*-(quinolin-8-yl)benzamide **1a** as the limiting reagent and 1-(pyrimidin-2-yl)-1*H*-indole **2a** as the coupling partner. Under the catalytic system comprising 20 mol% $Co(OAc)_2{\cdot}4H_2O$, 30 mol% (*S*)-Salox ((***S***)-**L1**) as the chiral ligand, 10 mol% Na_2EosinY as the photocatalyst, and 2.0 equiv NaOPiv as the additive in 2,2,2-trifluoroethanol (TFE), and irradiation with white LED bulbs (7 W × 4) for 36 h, the dearomatized product **3aa** was obtained in 45% yield with 79% *ee* as a single regioisomer (entry 1). The structure of **3aa** was confirmed through *X*-ray crystallographic analysis, and its absolute stereochemistry was assigned as (*R*,*R*)-configuration.[40]

Table 1. Reaction optimization[a]

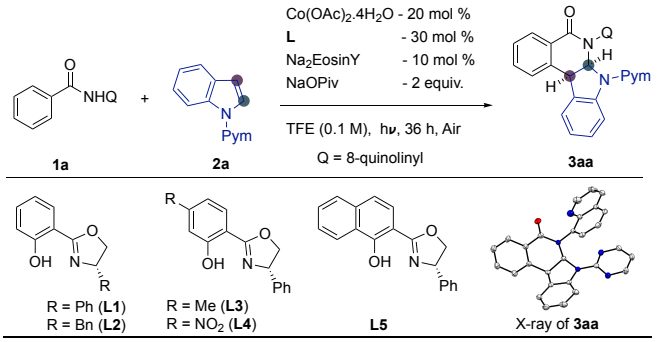

Entry	L	Base	Solvent	Yield (%)[b]	*ee* (%)[c]
1	(*S*)-L1	NaOPiv	TFE	45	79
2	(*S*)-L1	NaOPiv	EtOH	n.d.	n.d.
3	(*S*)-L1	NaOPiv	HFIP	25	59
4	(*S*)-L1	NaOPiv	^{t}BuOH	n.r.	n.d.
5	(*S*)-L2	NaOPiv	TFE	55	24
6	(*S*)-L3	NaOPiv	TFE	33	92
7	(*S*)-L4	NaOPiv	TFE	n.d.	n.d.
8	(*S*)-L5	NaOPiv	TFE	85	95
9	(*S*)-L5	PivOH	TFE	22	48
10	-	NaOPiv	TFE	n.r.	n.d.
11	(*S*)-L5	-	TFE	n.r.	n.d.
12	(*S*)-L5	NaOPiv	TFE	n.r.	n.d.[d]
13	(*S*)-L5	NaOPiv	TFE	n.r.	n.d.[e]
14	(*S*)-L5	NaOPiv	TFE	n.r.	n.d.[f]
15	(*S*)-L5	NaOPiv	TFE	n.r.	n.d.[g]
16	(*S*)-L5	NaOPiv	TFE	89	97[h]
17	(*S*)-L5	NaOPiv	TFE	71	91[i]
18	(*R*)-L5	NaOPiv	TFE	61	95[j]

[a] All reactions were carried out under air unless otherwise stated using **1a** (0.1 mmol), **2a** (0.15 mmol),$Co(OAc)_2{\cdot}4H_2O$ (20 mol%), Na_2EosinY (10 mol%), Salox **L** (30 mol%), and NaOPiv (0.20 mmol) in TFE (1.0 mL) under irradiation for 36 h. [b] Isolated yield. [c] The *e.e.* values were determined by chiral HPLC analysis. [d] without $Co(OAc)_2{\cdot}4H_2O$ [e] without Na_2EosinY [f] Performed under argon. [g] Performed under dark. [h] Performed with $Mn(OAc)_2.4H_2O$ (0.1 mmol) as oxidant at room temperature.[i] Performed in 1.0 mmol scale. [j] (*S*,*S*)-**3aa** was obtained with (*R*)-**L5**. TFE-2,2,2-Trifluoroethanol, n.r. = no reaction, n.d. = not determined.

To optimize the reaction conditions, we conducted systematic screenings of various solvents and chiral Salox ligands (entries 2–8). Among the solvents tested, TFE was found to be optimal, yielding the expected product **3aa** with moderate yields and good *ee* (entries 1-4). Considering the significant role of the Salox ligand in the reaction, we explored different ligand modifications to enhance both yield and enantiomeric excess (entries 5-8). Through quick screening of stereo-electronically biased Salox ligands (*S*)-**L2** – (*S*)-**L5**, (*S*)-**L5** emerged as the most promising ligand, affording an *ee* of up to 95% and a yield of 85% (entry 8).

Further fine-tuning of sodium pivalate to pivalic acid did not improve the yield or *ee*, suggesting that cobaltacycle formation is assisted by the carboxylate base (entry 9). Control experiments were conducted to elucidate the role of each parameter in the dearomatization protocol (entries 10-15). The absence of cobalt salt, Salox ligand, or base hindered the reaction, indicating their essential role in the activation and functionalization of the C-H bond (entries 10-12). Furthermore, without Na_2EosinY, no product formation was observed, highlighting the crucial role of the photocatalyst in oxidizing the cobalt (entry 13). An experiment conducted under argon or in the dark condition demonstrated the necessity of irradiation for product formation and the role of air/oxygen (entries 14-15). To compare the results, the similar reaction was setup with Mn(III) as oxidant at room temperature under standard conditions resulted in 89% isolated yield of **3aa** (*R*,*R*) with 98% *ee* (entry 16). To validate the practicality of the developed protocol, a 1.0 mmol scale reaction was performed, yielding the dearomatized product **3aa** with 71% yield and 91% *ee* (entry 17). Additionally, we tested other bidentate directing groups such as pyridine, benzoxazole, and aza-indole, but found them unsuitable under the reaction conditions (see the supporting information)[40]. Employing (*R*)-**L5** ligand instead of the (*S*)-variant resulted in the formation of the opposite isomer of **3aa**, i.e. (*S*,*S*)-**3aa**, in 61% yield with 95% *ee.*[40]

Upon employing optimized conditions, we initiated an exploration into the scope of benzamides, as delineated in Scheme 2. A diverse range of benzamides, featuring both *para*- and *meta*-substitutions, exhibited broad functional group tolerance and afforded the dearomatized annulated products in good-to-excellent yields and excellent enantioinduction. Substitutions encompassing various electron-donating (Me-, ^{t}Bu, MeO, OBn) and electron-withdrawing (CF_3, F, Cl, Br, Ph, OCF_3, SMe, CO_2Me, COMe) groups (**1b**–**1n**) at the *para*-position demonstrated suitability for the dearomatization process, yielding products within the range of 52% to 82%, and enantiomeric excess (*ee*) values spanning from 92% to >99%. In the case of meta-substituted benzamides, annulation favoured at the less hindered site, furnishing products (**3oa**–**3ra**) with yields ranging from 72% to 83% and *ee* values spanning from 92% to >99%. More interestingly, aromatic arene containing strong coordinating group such as sulphur group in 2-thienyl at the *para*-position is tolerable and provide the expected product **3sa** in good yield and 95% *ee*. Even naphthyl, thiophene based amides were also amenable and provide the annulated compound in 84% and 70% yield with >99% and 97% ee respectively. Validation of the stereochemistry and structural elucidation of **3qa**, **3oa**, and **3ua** was achieved through X-ray crystallography.[40]

We next examined the suitability of various stereo-electronically biased *N*-pyrimidyl indole derivatives under optimized reaction conditions (Scheme 3). A broad spectrum of electron-donating and electron-withdrawing functional groups, such as -OMe, -Me, NR_2, and -CO_2Me, -Br, -Ar positioned at the C-4, C-5 and C-6 sites of indole, exhibited excellent tolerance, affording the desired products (**3ab-3am)** in moderate-to-good yields (62-85%) with enantioinduction ranging from 86 to >99%. Notably, reactions involving substrates bearing sensitive and synthetically useful functional groups such as -F (**2m**), -Cl (**2k**), -Br (**2c**), and -OBn (**2h**) proceeded smoothly, and the resultant products were available for further derivatizations. Indoles featuring sterically hindered phenyl (**2e**, **2l**) and naphthyl (**2g**) moieties were also found to be compatible, providing the target

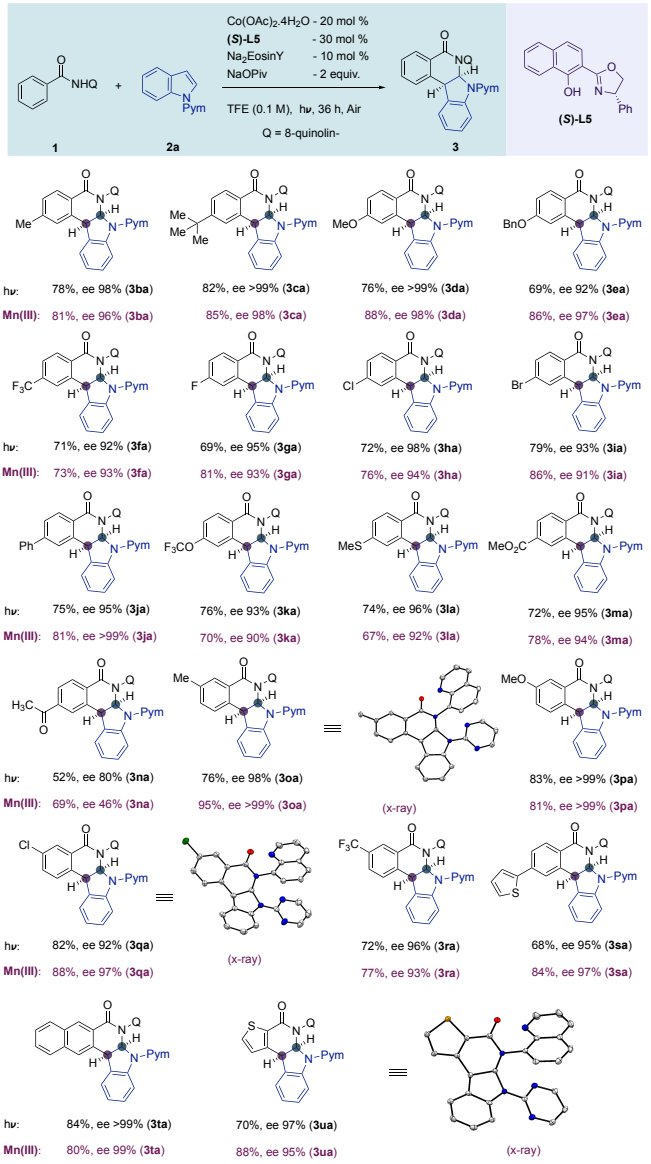

Scheme 2. Scope of aryl amides. The products obtained at room temperature (28-30 °C) using **1** (0.1 mmol), **2a** (0.15 mmol),$Co(OAc)_2{\cdot}4H_2O$ (20 mol%), Salox **L** (30 mol%), $Mn(OAc)_2{\cdot}4H_2O$ (0.1 mmol) and NaOPiv (0.20 mmol) in TFE (1.0 mL) for 36 h.

products in good yields (62-79% yield, 92->99% ee, respectively). Furthermore, to validate the protocol's applicability, biologically relevant indole **1f** was subjected to the optimized conditions, yielding the desired product **3af** in good yield (70%) and with high enantiopurity (95% *ee*). The scope of aryl amides and indole were also performed using Mn(III) as oxidant at room temperature (without Photocatalyst and no irradiation), and their results were given in scheme **2** and **3** for comparison.

Following the scope of our experimental work, we conducted a series of control experiments and Density Functional Theory (DFT) calculations aimed at elucidating the mechanistic underpinnings of the asymmetric dearomative coupling of indole with aryl amides, as depicted in Scheme 4. Initially, our objective was to isolate the crucial chiral octahedral cobaltacycle intermediate implicated in the catalytic cycle. The predominant

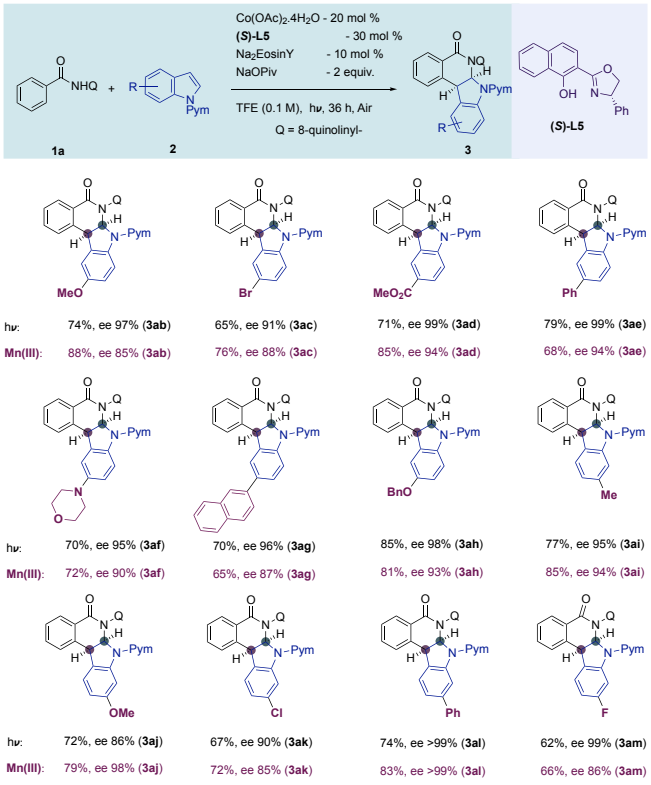

Scheme 3. Scope of Indole. The products obtained from at room temperature (28-30 ºC) using **1** (0.1 mmol), **2a** (0.15 mmol),$Co(OAc)_2{\cdot}4H_2O$ (20 mol%), Salox (*S*)-**L** (30 mol%), $Mn(OAc)_2.4H_2O$ (0.1 mmol) and NaOPiv (0.20 mmol) in TFE (1.0 mL) for 36 h.

diastereomer of the in situ-formed octahedral cobaltacycle, denoted as *mer*-[(***S***$_L$)-Δ$_{Co}$], was successfully isolated in 39% yield utilizing benzamide **1a** with $Co(OAc)_2{\cdot}4H_2O$, (*S*)-**L5**, NaOPiv, Na_2EosinY, and 4-acetylpyridine in 2,2,2-trifluoroethanol (TFE) under air atmosphere for 36 hours (Scheme 4a). The structure and stereochemistry of *mer*-[(***S***$_L$)-Δ$_{Co}$] were corroborated *via* X-ray crystallography. Subsequently, employing the isolated cobaltacycle *mer*-[(***S***$_L$)-Δ$_{Co}$] in a stoichiometric reaction with *N*-pyrimidyl indole furnished the desired product **3aa** in 70% yield with 92% enantiomeric excess (*ee*) (Scheme 4b). Furthermore, catalytic utilization of the octahedral cobaltacycle *mer*-[(***S***$_L$)-Δ$_{Co}$] engendered the desired annulation product **3aa** in 21% yield with 85% ee (Scheme 4c). Both catalytic and stoichiometric experiments corroborated the involvement of the cobaltacycle *mer*-[(***S***$_L$)-Δ$_{Co}$] in the catalytic cycle. To gain insights into the reaction pathway, we conducted the standard reaction in the presence of radical scavengers such as TEMPO and BHT, resulting in a significant reduction in product yield (10% and 12%, respectively), indicative of single electron transfer involvement during the catalytic cycle (see the supporting information)[41]. Furthermore, supplementation of the reaction mixture with 1.0 equiv. of DABCO did not affect the product yield, suggesting the absence of singlet oxygen during the reaction (Scheme 4d). To preclude the potential formation of superoxide anion *via* the photoredox process, the standard reaction was conducted in the presence of KO_2 under argon atmosphere, yielding only trace amounts of the desired product **3aa**, thus indicating that in-situ-generation of O_2^- is insufficient to re-oxidize the low-valent cobalt species (Scheme 4e).

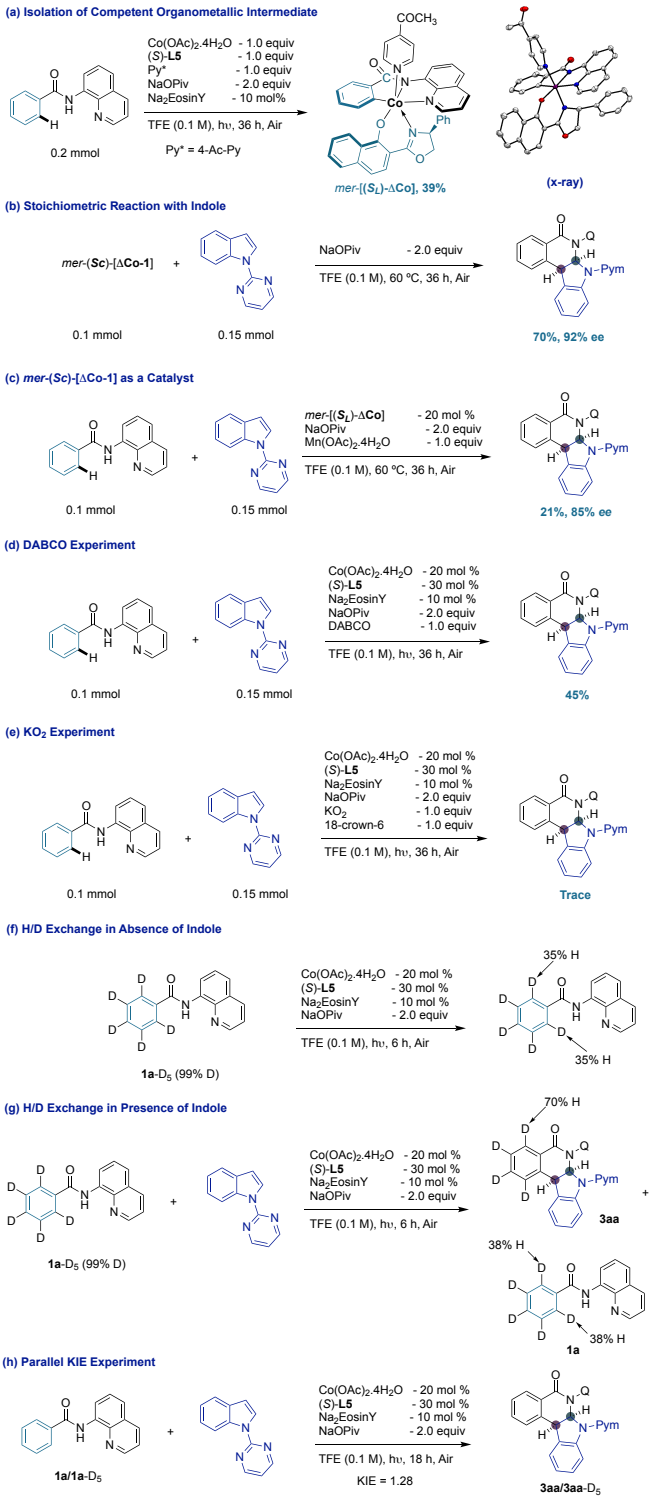

Scheme 4. Mechanistic studies and control experiments.

Subsequently, an intramolecular competitive experiment was conducted between electron-donating (**1o**) and electron-withdrawing (**1r**) substituents at the C-3 position of benzamide. Analysis revealed that substrate **1o** exhibited faster reactivity compared to **1r**, suggesting C–H bond activation occurs *via* Base-Induced Electrophilic Substitution (BIES) pathway.[41]

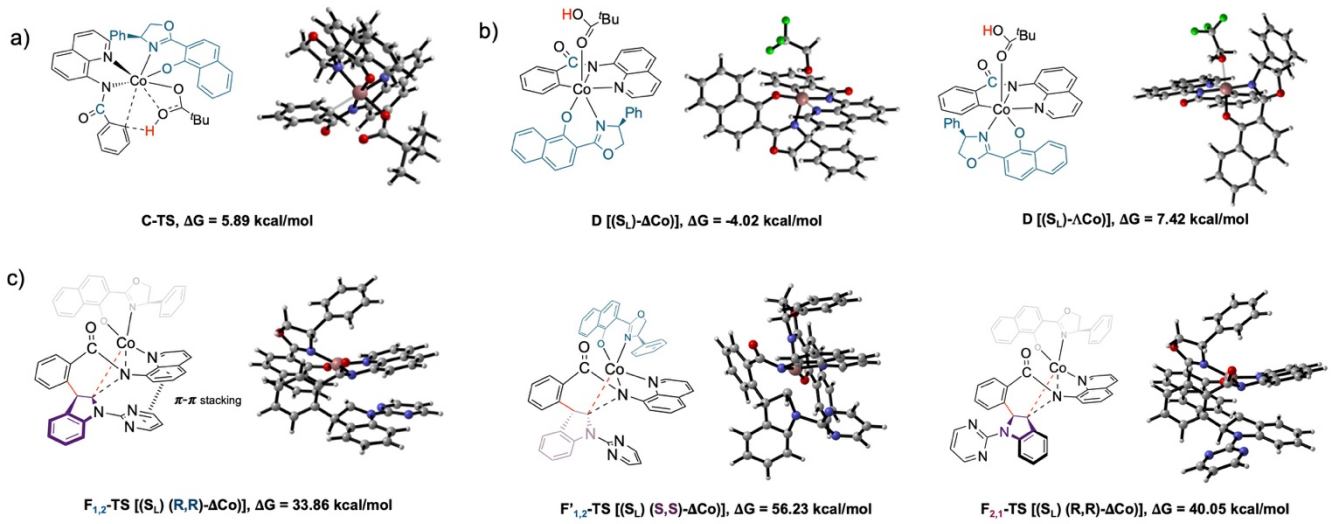

Figure 1. DFT calculations on (a) enantiodetermining C-H activation, (b) optimized structures for *mer*-[(***S*L**)-**ΔCo]** and *mer*-(***S*L**)-Λ**Co**] and (c) TS of the reductive elimination step.

Additionally, D/H scrambling experiments employing [D5]-**1a** in the absence and presence of *N*-pyrimidyl indole indicated significant D/H exchange at the ortho C-H bond in the recovered benzamide and annulated product, indicative of reversible C-H activation and involvement of the concerted metalation-deprotonation (CMD) pathway in the catalytic cycle (Scheme 4f & 4g). Moreover, a kinetic isotope effect value of 1.08 suggested that the C-H bond cleavage step of benzamide is not the rate-determining step (Scheme 4h).

DFT Studies

Quantum chemical investigations using density functional theory (DFT) were performed to gain further insights into reaction mechanism and the key energetics were depicted in Figure 1. The reference point for our calculations was [(*N,N*-**1a**)(***S*L**)Co^{III}(κ^2-Piv)],[41] with a transition state energy of 5.89 kcal/mol required to surpass the carboxylate-assisted concerted-metalation and deprotonation step. Upon C-H activation, multiple diastereomers are feasible. However, since the crystal structure confirmed meridional coordination modes as the geometrical isomer for the isolated cobalt complex, we did not compute the energy difference between these geometrical isomers. Given the fixed stereochemistry of the ligand with the use of enantiopure Salox ligand (***S***)-**L5**, we proceeded to evaluate the energy difference between the two principal optical isomers (Δ**Co**/Λ**Co**). Upon cyclocobaltation, this analysis revealed a disparity of 11.44 kcal/mol, favoring the intermediate *mer*-[(***S*L**)-Δ**Co**]. Subsequent substitution of pivalic acid with TFE in intermediate **D** demonstrated an energy barrier of 8.91 kcal/mol between the two optical isomers, thus reinforcing the superior stability of *mer*-[(***S*L**)-Δ**Co**].

Upon ligand exchange with indole in intermediate **D**, two stereoisomers *mer*-[(***S*L**)(***R,R***)-Δ**Co**] and *mer*-[(***S*L**)(***S,S***)-Δ**Co**]) were formed depending on the orientation of the indole during migratory insertion. The transition state energy difference between these orientations was found to be 4.96 kcal/mol. In the subsequent reductive elimination of intermediate **F** must pass through the transition state with the energy barrier of 33.87 kcal/mol for *mer*-[(***S*L**)(***R,R***)-ΔCo] and 50.68 kcal/mol for mer-[(***S*L**)(***S,S***)-ΔCo], favoring **3aa**-(***R,R***) under the reaction conditions. The stabilization of $F_{1,2}$-TS, *mer*-[(***S*L**)(***R,R***)-ΔCo], was evident through π-π stacking between the pyrimidine ring and arene of the 8-aminoquinoline. These computational results align with our experimental outcomes, further confirmed by *X*-ray analysis of the isolated dearomatized annulation products (**3aa, 3qa**, **3oa**, and **3ua**), establishing its absolute configuration as (***R,R***). Finally, the energy barrier for the 2,1-migratory insertion followed by reductive elimination was found to be 6.19 kcal/mol higher in energy compared to 1,2-migratory insertion, consistent with the experimental results as observed only 1,2-migratory insertion product from the reaction mixture. Overall, the energy profile suggests that reductive elimination, rather than C-H activation, is the rate-determining step, consistent with our experimental observations.

Drawing upon control experiments, stoichiometric studies, and DFT investigations, a plausible mechanistic pathway has been delineated, as shown in Scheme 5. [36b],[38-39] Initially, intermediate **B** is formed through sequential ligand exchange between $Co(OAc)_2{\cdot}4H_2O$, (***S***)-Salox ligand, and benzamide **1a**, followed by one-electron oxidation yielding Co(III) intermediate **C**. Photoexcited Na_2Eosin Y* facilitates the oxidation of Co(II) to Co(III), generating a radical anion of Na_2Eosin Y as a potent reductant. This species may then reduce triplet oxygen present in the reaction, completing a parallel catalytic cycle. Subsequently, carboxylate-assisted enantiodetermining C-H activation provides the diastereoselective *mer*-[(***S*L**)-Δ**Co**] cobaltacycle **D**. Upon coordination with the π-bond of the pyrrole ring in the indole molecule, intermediate **D** undergoes subsequent regioselective insertion between Co-C, stabilized by π-π stacking of the pyrimidine ring with the arene of the quinoline, yielding intermediate **F**. Further, reductive elimination from intermediate **F** and subsequent ligand exchange leads to the formation of the desired product **3aa** and liberated Co(I) species subsequently couples with benzamide **1a**, followed by oxidation mediated by the photocatalyst, regenerating the Cobalt intermediate **B**.

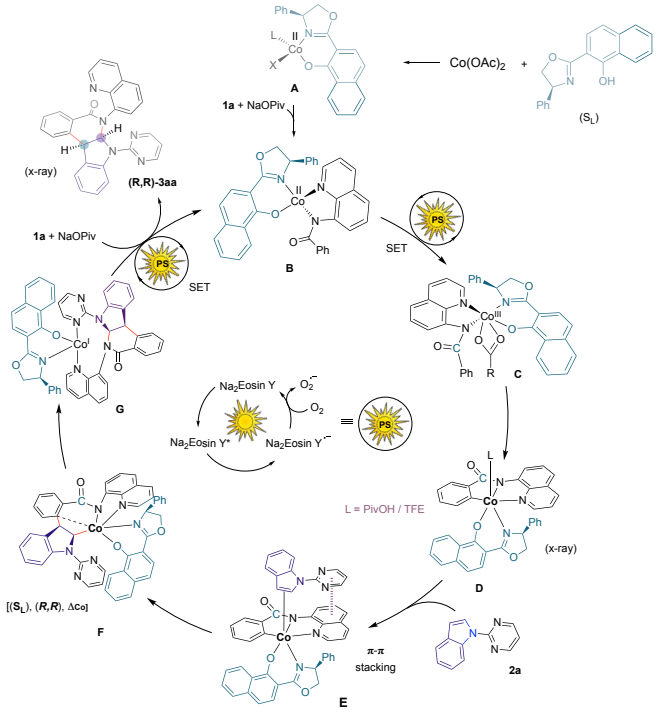

Scheme 5. Proposed mechanism.

Conclusion

In summary, we demonstrate the pioneering example of cobalt-catalyzed asymmetric dearomatization reaction *via* cascade C-H activation, leveraging the π-bond present in indole to access enantioenriched three-dimensional cyclic scaffolds in a single step under mild conditions. Notably, the developed method operates without the need for a metal oxidant, relying solely on oxygen as the oxidant and employing an organic dye as a photocatalyst under irradiation. Exploration of the scope of amides and indoles involved an examination of the tolerance of various functional groups under the established conditions. Control experiments and stoichiometric studies indicate that the enantiodetermining step is the C-H activation, which is reversible, though not rate-determining. Ongoing efforts in our laboratory are directed towards further harnessing this dual cobalt-photocatalytic approach for asymmetric functionalizations, promising to unveil novel synthetic methods and expand the repertoire of accessible chiral architectures.

Acknowledgements

Financial support provided by SERB (CRG/2020/001282) to support this research work is gratefully acknowledged. AD, SK and HSR acknowledges CSIR, IITK and PMRF for their fellowship.

Keywords: Dearomatization • C-H bond Functionalization • Cobalt • Indole • Photoredox • Asymmetric Catalysis

[1] R. Kaiser, *Angew. Chem., Int. Ed. Engl.* **1968**, *7*, 345−350.
[2] C. Zheng, S.-L. You, *ACS Cent. Sci.* **2021**, *7*, 432−444.
[3] W. C. Wertjes , E. H. Southgate and D. Sarlah, *Chem. Soc. Rev.*, **2018**, *47* , 7996−8017.
[4] C. J. Huck and D. Sarlah, *Chem*, **2020**, *6* , 1589−1603.
[5] C. Zheng, S.-L. You, *Chem*. **2016**, *1*, 830−857.
[6] P. V. R. Schleyer, H. Jiao, *Pure Appl. Chem.* **1996**, *68*, 209−218.
[7] M. Randic, *Chem. Rev.* **2003**, *103*, 3449−3606.
[8] Y. Hua, H. Zhang, H. Xia, *Chin. J. Org. Chem*. **2018**, *38*, 11−28.
[9] D. Astruc, Ed. Modern Arene Chemistry: Concepts, Synthesis,and Applications; Wiley-VCH, 2002.
[10] J. Mortier, Ed. Arene Chemistry: Reaction Mechanisms and Methods for Aromatic Compounds; Wiley-VCH, 2015.
[11] S. P. Roche, J. A. Porco. Jr. *Angew. Chem. Int. Ed*. **2011**, *50*, 4068-4093.
[12] C. Zheng, S.-L. You, *Nat. Prod. Rep*. **2019**, *36*, 1589-1605.
[13] A. J. Birch, *Pure Appl. Chem.* **1996**, *68*, 553-556.
[14] M. M. Heravi, M. V. Fard, Z. Faghihi, *Curr. Org. Chem*. **2015**, *19*, 1491-1525.
[15] B. K. Peters, K. X. Rodriguez, S. H. Reisberg, S. B. Beil, D. P. Hickey, Y. Kawamata, M. Collins, J. Starr, L. Chen, S. Udyavara, K. Klunder, T. J. Gorey, S. Anderson, M. Neurock, S. D. Minteer, P. S. Baran, *Science* **2019**, *363*, 838−845.
[16] A. Chatterjee, B. König, *Angew. Chem. Int. Ed*. **2019**, *58*, 14289-14294.
[17] K. Kondo, K. Kubota, H. Ito, *Chem. Sci.* **2024**, DOI: 10.1039/D3SC06052G.
[18] Selected examples using Hydrogenation: a) M. Heitbaum, R. Fröhlich, F. Glorius, *Adv. Synth. Catal*. **2010**, *352*, 357–362; b) Y. Wei, B. Rao, X. Cong, X. Zeng, *J. Am. Chem. Soc*. **2015**, *137*, 9250–9253; c) R. Kuwano, R. Morioka, M. Kashiwabara, N. Kameyama, *Angew. Chem., Int. Ed*. **2012**, *51*, 4136–4139; d) M. P. Wiesenfeldt, Z. Nairoukh, W. Li, F. Glorius, *Science* **2017**, *357*, 908–912.
[19] Selected examples on Dearomatization: a) Y. Schmidt, J. K. Lam, H. V. Pham, K. N. Houk, C. D. Vanderwal, *J. Am. Chem. Soc*. **2013**, *135*, 7339–7348. b) W. B. Motherwell, A. S. Williams, *Angew. Chem., Int. Ed. Engl*. **1995**, *34*, 2031–2033. c) B. M. Trost, V. Ehmke, B. M. O'Keefe, D. A. Bringley, *J. Am. Chem. Soc*. **2014**, *136*, 8213–8216. d) J. Ling, S. Lam, K.-H. Low, P. Chiu, *Angew. Chem., Int. Ed*. **2017**, *56*, 8879–8882. e) G. Jacquemot, M.-A. Ménard, C. L'Homme, S. Canesi. *Chem. Sci*. **2013**, *4*, 1287–1292. f) S. E. Reisman, R. R. Nani, S. Levin. *Synlett* **2011**, 2437–2442.
[20] S. E. Lewis, S.-L. You, Ed. Wiley-VCH. **2016**; pp 279-346.
[21] Q. Cheng, Y. Wang, S.-L. You. *Angew. Chem., Int. Ed.* **2016**, *55*, 3496–3499.
[22] H.-F. Tu, C. Zheng, R.-Q. Xu, X.-J. Liu, S.-L. You. *Angew. Chem., Int. Ed*. **2017**, *56*, 3237–3241.
[23] D. Shen, Q. Chen, P. Yan, X. Zeng, G. Zhong. *Angew. Chem., Int. Ed*. **2017**, *56*, 3242–3246.
[24] M. Aleksiev, O. García Mancheño, *Chem. Commun*. **2023**, *59*, 3360-3372.
[25] C.-X. Zhuo, C. Zheng, S.-L. You, *Acc. Chem. Res*. **2014**, *47*, 2558-2573.
[26] a) M. Okumura, D. Sarlah, D. *Synlett* **2018**, *29*, 845–855. b) K. Ikeda, R. Kojima, K. Kawai, T. Murakami, T. Kikuchi, M. Kojima, T. Yoshino, S. Matsunaga, *J. Am. Chem. Soc*. **2023**, *145*, 9326–9333. c) S. Pradhan, F. Mohammadi, J. Bouffard, *J. Am. Chem. Soc.* **2023**, *145*, 12214–12223.
[27] J. Zheng, S.-B. Wang, C. Zheng, S.-L. You, *J. Am. Chem. Soc*. **2015**, *137*, 4880–4883.
[28] C. Zheng, J. Zheng, S.-L. You, *ACS Catal.* **2016**, *6*, 262–271.
[29] X. Li, L. Hu, S. Ma, H. Yu, G. Lu, T. Xu, *ACS Catal*. **2023**, *13*, 4873.
[30] L. Grigorjeva, O. Daugulis, *Angew. Chem., Int. Ed*. **2014**, *53*, 10209-10212.
[31] a) Y. Kommagalla, N. Chatani, *Coord. Chem. Rev*. **2017**, *350*, 117–135. b) L. Lukasevics, A. Cizikovs, L. Grigorjeva, *Chem. Commun*., **2021**, *57*, 10827–10841. c) A. Baccalini, S. Vergura, P. Dolui, G. Zanoni, D. Maiti, *Org. Biomol. Chem*. **2019**, *17*, 10119–10141. d) R. Mandal, B. Garai, B. Sundararaju. *Science of Synthesis*. **2023**, *2*, 149-260.
[32] (a) P. Gandeepan, L. H. Finger, T. H. Meyer, L. Ackermann, *Chem. Soc. Rev*. **2020**, *49*, 4254-4272. (b) V. Dwivedi, D. Kalsi and B. Sundararaju. *ChemCatChem*. **2019**, *11*, 5160-5187. (c) L. Guillemard, J. Wencel-Delord. *Beilstein J. Org. Chem*. **2020**, *16*, 1754–1804. (d) P. Chakraborty, R. Mandal, S. Paira, B. Sundararaju. *Chem. Commun*. **2021**, *57*, 13075-13083.

[33] A. Cizikovs, L. Grigorjeva, *Inorganics*, **2023**, *11*, 194.

[34] a) Y. Zheng, C. Zheng, Q. Gu and S.-L. You, *Chem. Catal.*, **2022**, *2*, 2965–2985; (b) B. Garai, A. Das, D. Vineet Kumar, B. Sundararaju. *Chem. Commun.*, **2024**, *60*, 3354-3369. c) X. Yu, Z.-Z. Zhang, J.-L. Niu and B.-F. Shi, *Org. Chem. Front.*, **2022**, *9*, 1458–1484.

[35] Selected reviews on enantioselective C-H bond functionalizations with 3d metals, see: a) Ł. Woźniak, N. Cramer, *Trends Chem.* **2019**, *1*, 471–478. b) J. Loup, U. Dhawa, F. Pesciaioli, J. Wencel-Delord, L. Ackermann, *Angew. Chem. Int. Ed.* **2019**, *58*, 12803–12818. c) R. Mandal, B. Garai, B. Sundararaju, *ACS Catal.* **2022**, *12*, 3452–3506. d) T. Yoshino, *Bull. Chem. Soc. Jpn.* **2022**, *95*, 1280–1288. e) T. Yoshino, S. Matsunaga, *Synlett* **2019**, *30*, 1384–1400.

[36] a) X.-J. Si, D. Yang, M.-C. Sun, D. Wei, M.-P. Song, J.-L. Niu, *Nat. Synth.* **2022**, *1*, 709–718. b) Q.-J. Yao, F.-R. Huang, J.-H. Chen, M.-Y. Zhong, B. F. Shi, *Angew. Chem. Int. Ed.* **2023**, *62*, e202218533. c) D. Yang, X. Zhang, X. Wang, X.-J. Si, J. Wang, D. Wei, M.-P. Song, J.-L. Niu, *ACS Catal.* **2023**, *13*, 4250-4260. d) Z.-K. Wang, Y.-J. Wu, Q.-J. Yao, B.-F. Shi, *Angew. Chem. Int. Ed*. **2023**, *62*, e202304706. e) T. Li, L. Shi, X. Wang, C. Yang, D. Yang, M.-P. Song, J.-L. Niu, *Nat. Commun*. **2023**, *14*, 527. f) Y.-J. Wu, J.-H. Chen, M.-Y. Teng, X. Li, T.-Y. Jiang, F.-R. Huang, Q.-J. Yao, B.-F. Shi, *J. Am. Chem. Soc*. **2023**, *145*, 24499-24505. g) Y.-J. Wu, Z.-K. Wang, Z.-S. Jia, J.-H. Chen, F.-R. Huang, B.-B. Zhan, Q.-J. Yao, B.-F. Shi, *Angew. Chem. Int. Ed.* **2023**, *62*, e2023100. h) Y. Lin, T. von Münchow, L. Ackermann, *ACS Catal.* **2023**, *14*, 9713–9723. i) M.-Y. Teng, Y.-J. Wu, J.-H. Chen, F.-R. Huang, D.-Y. Liu, Q.-J. Yao, B.-F. Shi, *Angew. Chem. Int. Ed*. **2024**, *63*, e2023188.

[37] a) Q.-J. Yao, J.-H. Chen, H. Song, F.-R. Huang, B.-F. Shi,. *Angew. Chem. Int. Ed*. **2022**, *61*, e202202892. b) J.-H. Chen, M.-Y. Teng, F.-R. Huang, H. Song, Z.-K. Wang, H.-L. Zhuang, Y.-J. Wu, X. Wu, Q.-J. Yao, B.-F. Shi, *Angew. Chem. Int. Ed*. **2022**, *61*, e202210106. c) T. von Münchow, S. Dana, Y. Xu, B. Yuan, L. Ackermann, *Science* **2023**, *379*, 1036–1042. d) G. Zhou, J.-H. Chen, Q.-J. Yao, F.-R. Huang, Z.-K. Wang, B.-F. Shi, *Angew. Chem. Int. Ed*. **2023**, *62*, e202302964. e) T. Liu, W. Zhang, C. Xu, Z. Xu, D. Song, W. Qian, G. Lu, C.-J. Zhang, W. Zhong, F. Ling, *Green Chem.*, **2023**, *25*, 3606-3614. f) A. Das, R. Mandal, H. S. Ravi sankar, S. Kumaran, D. Borah, J. R. Premkumar, B. Sundararaju, *Angew. Chem. Int. Ed*. **2024**, *63*, e202315005.

[38] a) D. Kalsi, S. Dutta, N. Barsu, M. Rueping, B. Sundararaju, *ACS Catal.* **2018**, *8*, 8115-8120. b) D. Kalsi, N. Barsu, S. Chakrabarti, P. Dahiya, M. Rueping and B. Sundararaju, *Chem. Commun.*, **2019**, *55*, 11626-11629. c) R. Mandal, N. Barsu, B. Garai, A. Das, D. Perekalin and B. Sundararaju, *Chem. Commun.*, **2021**, *57*, 13075-13083.

[39] Contribution from other research groups, see: a) Y.-L. Ban, L. You, T. Wang, L.-Z. Wu, Q. Liu, *ACS Catal*. **2021**, *11*, 5054-5060. b) S. Kumar, A. M. Nair, C. M. R. Volla, *Chem. Asian J*. **2022**, *17*, e202200801. c) N. P. Khot, N. K. Deo, M. Kapur, *Chem. Commun*, **2022**, *58*, 13967-13970. d) C. Sen, B. Sarvaiya, S. Sarkar, S. C. Ghosh, *J. Org. Chem*. **2020**, *23*, 15287-15304.

[40] CCDC 2344417 (**3aa**), 2344418 (**3oa**), 2344419 (**3qa**), 2344420 (**3ua**), and CCDC 2344416 *mer*-[(S_L)-ΔCo] contains the supplementary crystallographic data for this paper. These data can be obtained free of charge from The Cambridge Crystallographic Data Centre via www.ccdc.cam.ac.uk/data_request/cif. The Supporting Information also provides additional information.

[41] See the supporting information for more details.

Entry for the Table of Contents

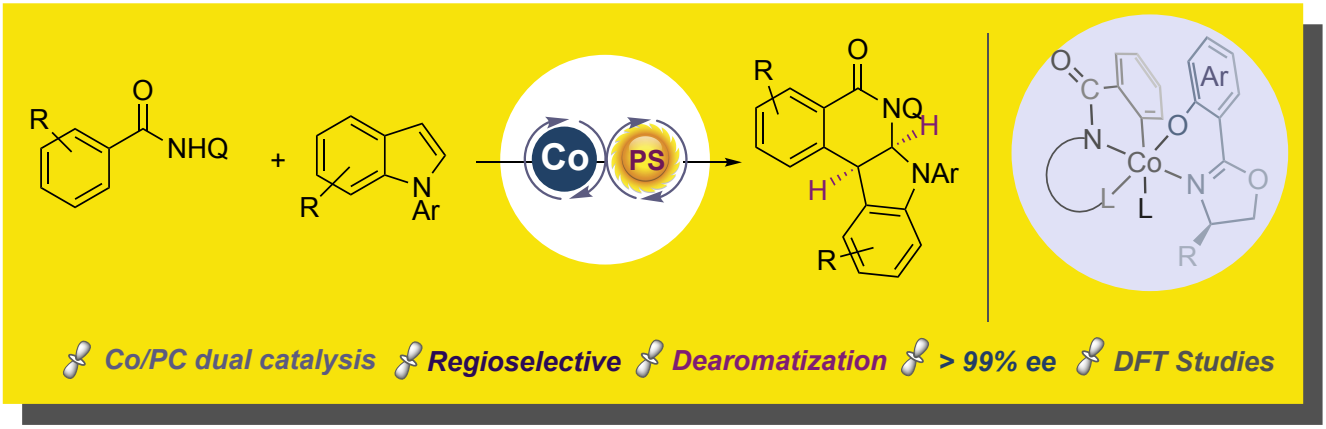

In this study, we showcase the successful cobalt-catalyzed asymmetric dearomatization of indoles with aryl amides, achieving remarkable enantioinduction and exceptional regioselectivity. This dual catalytic strategy, which integrates photocatalyst and cobalt, represents a pioneering approach in asymmetric C-H bond functionalization. Notably, this method offers a pathway to accessing chiral three-dimensional molecules. Through detailed experimental investigations and DFT calculations, we present a plausible mechanism to elucidate the reaction pathway.

Institute and/or researcher Twitter usernames: @basker25071980 @basker_IITK